Journal of Catalysis **210,** 273–284 (2002)
doi:10.1006/jcat.2002.3676

Reverse Topotactic Transformation of a Cu–Zn–Al Catalyst during Wet Pd Impregnation: Relevance for the Performance in Methanol Synthesis from CO_2/H_2 Mixtures

I. Melián-Cabrera, M. López Granados, and J. L. G. Fierro[1]

Instituto de Catálisis y Petroleoquímica, Consejo Superior de Investigaciones Cientificas, Campus Cantoblanco, 28049 Madrid, Spain

Received December 12, 2001; revised March 11, 2002; accepted May 8, 2002

The effect of palladium metal on the performance of a CuO–ZnO–Al_2O_3 catalyst is studied for methanol synthesis by hydrogenation of carbon dioxide. The dramatic decrease in the methanol yield (in mol $CH_3OH/h \cdot g_{cat}$) seen for the Pd-containing catalysts is discussed in terms of formation, decomposition, and reconstruction of hydroxycarbonate precursors. The CuO–ZnO–Al_2O_3 mixed oxide, obtained by calcination (673 K) of a hydrotalcite-containing precursor, still contains interlayer CO_3^{2-} anions as a result of incomplete decomposition. The presence of the remaining carbonate anion and the hydrothermal-like treatment during the Pd impregnation step allow the partial reconstruction of the original hydrotalcite-type structure. An improvement in the crystallinity of the copper oxide phase is also obtained. This improvement in crystallinity occurs during the hydrotalcite reconstruction and is a consequence of crystalline rearrangement of this oxidic phase. Such an effect gives rise to poorer copper dispersion and, consequently, to an apparent masking of the promoting effect of palladium. However, nitrous oxide chemisorption measurements allow the redefinition of the methanol yield per mole of exposed copper, a situation that clearly reveals the intrinsic promoting effect of palladium. The appearance of low-temperature reduction peaks involving Cu(II) species and the increase in the hydrogen consumption for the Pd-modified catalysts, both compared to the base CuO–ZnO–Al_2O_3 catalyst, indicate a hydrogen-spillover mechanism as being responsible for the intrinsic promoting effect of palladium.

Key Words: **Pd-modified catalysts; copper–zinc–aluminium catalysts; carbon dioxide hydrogenation; methanol synthesis; hydrotalcite reconstruction; hydrogen spillover; promoting effect; TPR; structure–activity relationship.**

1. INTRODUCTION

Methanol is currently produced from CO-rich synthesis gas ($CO/CO_2/H_2$) using a ternary Cu–Zn–Al oxide catalyst at 50–100 bar and 473–523 K (1). CO_2 is used as a carbon source for methanol synthesis based on the fact that kinetic experiments, using isotope-labelled carbon oxides (2, 3) and spectroscopic methods (4), have demonstrated that methanol is produced from hydrogenation of CO_2, whereby CO merely provides a source of CO_2 and acts as a reducing agent by scavenging surface oxygen. Nevertheless, the ternary catalyst that is active for CO-rich feedstock is not so active for CO_2-rich sources (5, 6). It has been shown that the water formed as a byproduct (reactions [1] and [2]) has an inhibitory effect on methanol synthesis because it tends to oxidise the active copper metal during reaction (7–9):

$$CO_2 + 3H_2 \rightleftarrows CH_3OH + H_2O \quad [1]$$

$$CO_2 + H_2 \rightleftarrows CO + H_2O. \quad [2]$$

In addition, it was reported that CO_2 keeps the copper surface partially oxidised during methanol synthesis (10, 11). Within this context, there have been many claims that the catalyst performance can be improved. The majority of the modified catalysts still contain Cu and Zn as the main components, together with different modifiers such as chromium (12), zirconium (13–15), vanadium (15), cerium (16), titanium (17, 18), and gallium (19, 20). One particularly attractive possibility is the incorporation of Group VIII noble metals within the catalytic system. The noble metals are excellent candidates to activate hydrogen, which could then spread over the neighbouring phases through a hydrogen-spillover mechanism. This process leads to a more reduced state for the catalyst surface, a situation that may further facilitate surface hydrogenation reactions. Methanol synthesis from a CO_2/H_2 feed has already been achieved by either physically mixing a CuO–ZnO catalyst with a Pd catalyst (7, 8) or by using Pd-impregnated CuO–ZnO–Al_2O_3 catalysts instead of physical mixtures (9). The enhancement of the catalytic activity for these Pd-modified materials was explained in terms of hydrogen spillover from metallic Pd to metallic Cu—the active component of the Cu-based catalyst.

In earlier research (21) we reported that the addition of palladium to a conventional CuO–ZnO–Al_2O_3 methanol synthesis catalyst led to an increase in the methanol yield, expressed per mole of exposed copper (determined by

[1] To whom correspondence should be addressed. Fax: 34 915854760. E-mail: jlgfierro@icp.csic.es.

0021-9517/02 $35.00

XPS). In spite of the promoting effect of palladium revealed in our previous work, there is still a lack of understanding in terms of the influence that the preparation method has on catalyst performance. In particular, the catalytic activity of the modified catalysts (defined per gram of catalyst) markedly decreases after impregnation. The aim of this continuing work was to perform a more detailed characterisation of Pd-modified precursors and calcined catalysts, as well as to investigate their relationship with the catalyst performance in the synthesis of methanol by direct hydrogenation of CO_2. Special care was taken to characterise the rehydration of the CuO–ZnO–Al_2O_3 mixed oxide during the Pd-impregnation step.

2. EXPERIMENTAL

2.1. Catalyst Preparation

The Cu–Zn–Al(CZA) precursor (Cu/Zn/Al = 55 : 30 : 15 atomic ratio) was prepared by coprecipitation at constant pH (ca. 7) and constant temperature (343 K) (22). A solution containing metal nitrates (Panreac, analytical grade) ($[Cu^{2+}] + [Zn^{2+}] + [Al^{3+}] = 1.0$ M) and a sodium carbonate solution (1.1 M) (Fluka, analytical grade) were simultaneously added to a reaction vessel containing a small amount of deionized water (18 MΩ/cm as supplied by a Millipore deionizer). The suspension was vigorously stirred and maintained at the desired pH by adjusting the relative flow rates of the two solutions. The final suspension was aged under stirring (343 K for 4 h) and cooled down to room temperature overnight. The precipitate was filtered off and repeatedly washed with sufficient deionized water to remove residual sodium (less than 0.5 ppm in mother liquid). The solid was dried overnight at 363 K (precursor) and calcined in air at 673 K for 4 h (catalyst). The resulting calcined powder (calcined CZA), besides being the reference catalyst, was used as the starting material in the preparation of the palladium-modified catalysts.

Two Pd-containing catalysts (4.0 and 10.0 Pd wt%) were prepared by impregnation of the base CZA catalyst with an aqueous solution of $Pd(NO_3)_2$ (Alfa Aesar, reagent grade). The details of the preparation method are described elsewhere (21). The samples, also calcined at 673 K, are denoted as XPd/CZA: where X is the nominal loading of palladium (wt%) in the calcined material and CZA represents the CuO–ZnO–Al_2O_3 mixed oxide.

2.2. Catalyst Characterisation

Thermal analyses of the CZA precursor were carried out with a Perkin-Elmer TGS-2 analyzer for thermogravimetric analysis (TGA) and a Baltzer Prisma quadrupole mass spectrometer (QMS 200) for evolved gas analysis (EGA-MS). The standard TGA protocol involved heating the sample (5–10 mg) under a flow of air (50 mL/min) at a rate of 10 K/min from ambient temperature to 1173 K. The gases evolved during the precursor decomposition were also analyzed online by a computer-controlled mass spectrometer. Samples (10–20 mg) were placed in a U-shaped quartz reactor incorporated within a flow system and connected to the mass spectrometer (QMS 200). Analyses were performed in a mixture of 21 vol% O_2 in Ar (50 mL/min) and the temperature was increased from room temperature to 1173 K at a heating rate of 10 K/min.

Elemental composition of the calcined catalysts was determined by inductively coupled plasma atomic emission spectroscopy (ICP-AES), using a Perkin-Elmer Optima 3300DV apparatus.

The powder X-ray diffraction patterns were obtained with a Seifert 3000 XRD diffractometer. All the samples were scanned using Cu $K\alpha$ (nickel-filtered) radiation in the range $10^\circ < 2\theta < 75^\circ$ in the step mode (0.02°, 2 s). The mean crystallite sizes (D) of CuO and ZnO were determined from the line broadening of the (111) ($2\theta = 38.77^\circ$) and (100) ($2\theta = 31.77^\circ$) diffraction lines for CuO and ZnO, respectively, using the Scherrer equation after correction for instrumental broadening ($D = K\lambda/\beta\cos\theta$ with $K = 0.9$).

The specific area of the calcined samples was determined by N_2 adsorption isotherms (77 K) in a Micromeritics TriStar apparatus, using the BET method. The samples were evacuated at 413 K overnight prior to N_2 dosage.

Temperature-programmed reduction (TPR) experiments were carried out in a semiautomatic Micromeritics TPD/TPR 2900 apparatus. Because the reduction profiles can be perturbed by experimental conditions (23, 24), the operating variables [initial amount of reducible oxide (S_o), total flow rate (V^*), heating rate (β), and the initial H_2 concentration (C_o)] were chosen in such a way that the line profile, peak position, and H_2 consumption could be measured accurately. TPR profiles were characterised by (i) the temperature at which maximum H_2 consumption was observed (T_M) and (ii) the ratio between the amount of H_2consumed and the amount of reducible oxide species present (H_2/M). The amount of hydrogen consumed during reduction was obtained after calibration of the thermal conductivity detector with pure copper oxide (Aldrich). Reduction of the CZA sample began at room temperature (ca. 298 K), whereas measurements were made on the Pd-containing samples starting at cryogenic temperatures (ca. 223 K). For the sake of comparison, pure CuO (Aldrich, reagent grade) was also studied as a reference compound.

The amount of exposed copper (copper surface area) was evaluated by dissociative nitrous oxide chemisorption

$$2Cu_{(S)} + N_2O_{(g)} \rightarrow Cu_2O_{(S)} + N_{2(g)} \qquad [3]$$

where $Cu_{(S)}$ denotes a surface copper atom. The procedure used was essentially similar to that reported by Evans *et al.* (25). The measurements were performed with

a Micromeritics TPD/TPR 2900 apparatus. The sample, positioned in a U-shaped quartz reactor, was first reduced at 553 K (1 h) in an H_2/N_2 mixture (10 vol%, 60 mL/min). After cooling the catalyst to 353 K (chemisorption temperature) with nitrogen, pulses of nitrous oxide (0.1 cm^3) were injected into the nitrogen line using a gas sampling valve. The consumption of N_2O was monitored by a thermal conductivity detector. The copper surface area was calculated assuming an atomic copper surface density of 1.46×10^{19}Cu atoms/m^2 (26) and a molar stoichiometry of N_2O/Cu = 0.5.

2.3. Catalytic Activity

Catalytic activity tests were carried out using a stainless-steel fixed-bed flow reactor and using different equipment and conditions than those given in previous work (21). The reaction was conducted at 40 bar overall pressure with a CO_2/H_2 mixture ($CO_2 : H_2 = 1:3$, molar) at a W/F value of 0.042 kg · h/m^3. The catalyst, diluted with SiC at a volume ratio of 3 : 1 to avoid thermal effects (hot spots), was placed in a tubular reactor (11-mm i.d.) with a coaxially centered thermocouple in contact with the catalytic bed. The addition of SiC diluent improves the heat conduction in the bed and decreases the effect of the axial dispersion in the catalyst bed. The catalyst particle size (D_p) used was between 0.4 and 0.5 mm, making the D_{CB}/D_p ratio (where D_{CB} is the diameter of the catalytic bed) higher than 20, thus avoiding the wall effects on the gas–solid operation. Moreover, the L_{CB}/D_p ratio (where L_{CB} is the length of the catalytic bed) was almost 40, due to the dilution of the catalyst with inert material, assuring a deviation of the plug-flow behaviour of less than 5%. Prior to reaction, the sample was reduced *in situ* at 553 K (heating rate 5 K/min) with a flow rate of 60 mL/min of a 10 vol% H_2/N_2 mixture for 2 h. The pretreatment gases were flushed from the reactor with N_2 before addition of the CO_2/H_2 mixture. Once the system reached the operating pressure, the reaction temperature was increased gradually (2 K/min). Activity was measured between 433 and 473 K, running from the lowest to the highest temperature and maintaining the reaction for 4 h at each temperature. The effluent from the reactor was analysed online using a Hewlett–Packard 5890 Series II gas chromatograph. The transfer line from the reactor to the chromatograph was heated at 423 K in order to avoid condensation of the reaction products. Although all the catalysts were very stable under reaction, steady-state values of CO_2 conversion were taken as the average of the five different analyses after onstream operation for 4 h at a given temperature. The activity of the catalysts was fairly constant with time onstream and the reproducibility of the measurements was within ±7% of the mean value. The carbon mass balance was more than acceptable (±5% difference between reactor input and output).

3. RESULTS AND DISCUSSION

3.1. Characterisation of the Base CZA Precursor

The XRD pattern of the CZA precursor is presented in Fig. 1 (graph A). The typical pattern of the Cu–Zn hydrotalcite-like structure [$Cu_2Zn_4Al_2(OH)_{16}CO_3 \cdot 4H_2O$] (27) can be detected in the base CZA precursor. Although the intensities of the two peaks at $2\theta \approx 32^\circ$ were difficult to index, the remaining diffraction peaks were assigned to a zincian–malachite phase [$(Cu, Zn)_2CO_3(OH)_2$] (28),

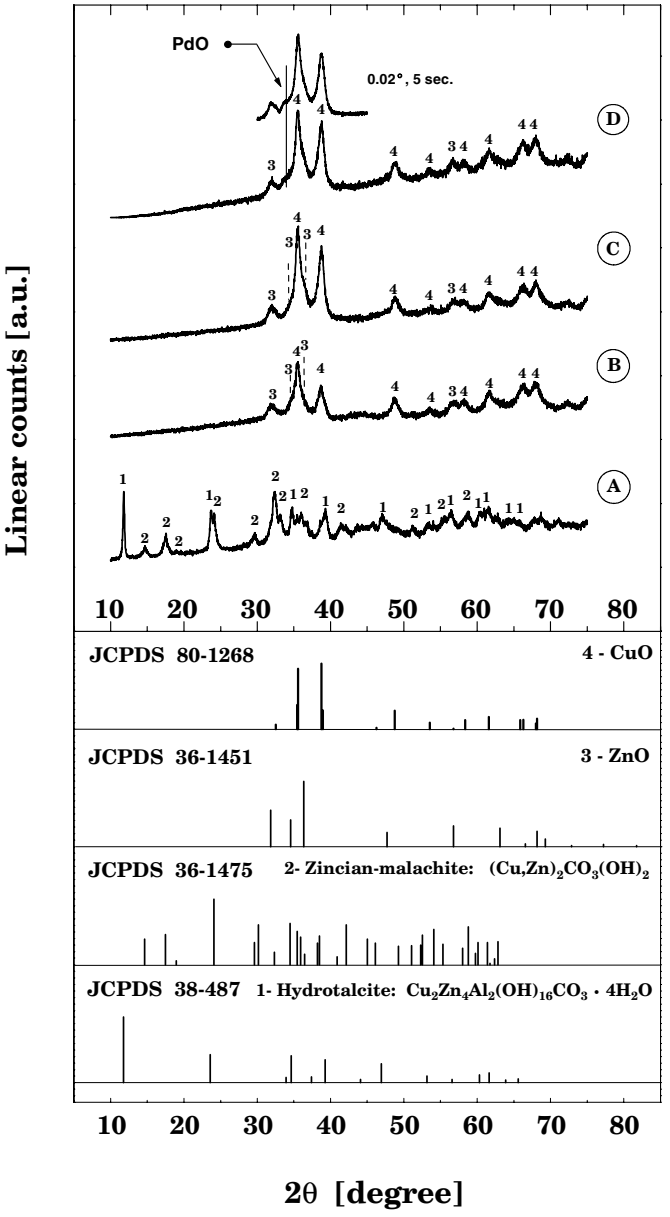

FIG. 1. X-ray powder diffraction profiles: (A) CZA precursor, (B) CZA calcined catalyst, (C) 4Pd/CZA, and (D) 10Pd/CZA modified catalysts.

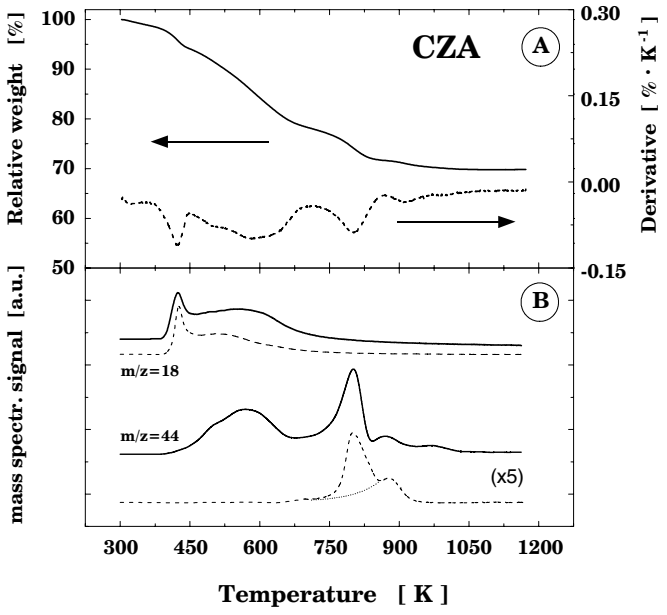

FIG. 2. (A) TGA curve (solid line) and derivative curve (dotted line) of the CZA precursor. (B) Mass spectrometry traces of H_2O ($m/z = 18$) and CO_2 ($m/z = 44$) for the CZA precursor (solid lines) and $Cu_2Zn_4Al_2(OH)_{16}CO_3 \cdot 4H_2O$ hydrotalcite as reference compound (dashed lines).

and this was supported by other work in the literature (22, 29).

The thermal decomposition of the CZA precursor studied by two methods is given in Fig. 2. The EGA-MS method involved detection of fragments at $m/z = 18$ (H_2O) and 44 (CO_2) with a quadrupole mass spectrometer (solid lines in Fig. 2, part B). The derivative of the TGA curve is also included in Fig. 2, part A (dotted line) to facilitate the interpretation. There is correspondence between the processes observed using TGA and those using MS detection.

The precursor underwent four weight losses upon heating under a flow of air. The first weight loss is associated with removal of the water of crystallisation present in the Cu–Zn hydrotalcite-like structure, which is clearly visible in the derivative TGA peak at ca. 440 K. A second broad peak at 570 K occurs due to H_2O and CO_2 co-evolution during decomposition of both hydroxycarbonate phases. Elimination of structural hydroxyl groups from both phases resulted in the formation of H_2O, but the evolution of CO_2 is due to the decomposition of the zincian–malachite only. Finally, the hydrotalcite carbonate groups decompose in the next two weight losses at higher temperatures (700–900 K). This indicates that below 673 K (the calcination temperature), the hydrotalcite CO_3^{2-} units remain occluded in the solid. The assignment of this peak to the decomposition of hydrotalcitic CO_3^{2-} groups is based on TGA and EGA-MS experiments of a $Cu_2Zn_4Al_2(OH)_{16}CO_3 \cdot 4H_2O$ hydrotalcite prepared according to the method described in the literature (29). This analysis showed (see dashed lines in Fig. 2, part B) H_2O evolution at 440 K (dehydration) and at 550 K (dehydroxylation), followed by CO_2 formation in the range 750–900 K resulting from carbonate decomposition.

3.2. Characterisation of the Calcined Samples

Palladium impregnation was carried out on a Cu–Zn–Al mixed oxide catalyst obtained by calcination (673 K) of the CZA precursor. The calcination temperature was selected as 673 K although the TGA and EGA-MS studies indicate incomplete decomposition of the precursor at this temperature. Higher calcination temperatures, as required to decompose the remaining CO_3^{2-} groups, were not used because they are close to the higher limit allowed to minimise thermal sintering of the CuO phase. Such sintering has a detrimental effect on the catalytic activity for the methanol synthesis reaction.

The metal compositions of the catalysts (wt%), as determined by ICP-AES, are given in Table 1. The composition values for the base CZA catalyst are slightly lower than the theoretical values (data between parentheses), a fact that could be attributed to incomplete decomposition of the Cu–Zn hydrotalcite phase, as indicated by TGA and EGA-MS studies. The remainder of CO_3^{2-} groups occluded in the structure, instead of O^{2-} anions, introduced a modified weight basis that was not considered in the calculation of the theoretical values. This situation leads to a systematic difference of ca. 5% between the experimental and theoretical values. In contrast, the experimental atomic ratio for the metals (Cu/Zn/Al = 54.9 : 29.7 : 15.4) is in very good agreement with the theoretical value (Cu/Zn/Al = 55 : 30 : 15) and confirms the diluting effect of the carbonate anions in the calculation of the composition for the oxidic phase. As far as the calcined Pd-containing catalysts are concerned, the palladium concentrations were also lower than expected, probably for the same reason. Removal of sodium by repeated washing with deionized water during catalyst preparation was successful because sodium was not detected by ICP-AES.

TABLE 1

Chemical Composition of Calcined Catalysts

	Chemical composition (wt%)				
Catalyst	Na	Pd	Cu	Zn	Al
CZA[a]	—	—	43.8 (46.1)	24.4 (25.6)	5.2 (5.5)
4Pd/CZA	—	3.7	42.2	23.3	4.8
10Pd/CZA	—	9.2	40.0	21.6	4.0

Note. The symbol (—) indicates that the values are under the detection limit of the ICP-AES technique.

[a] Values in parentheses represent the theoretical composition (metal wt%) for a catalyst with an atomic ratio of Cu/Zn/Al = 55 : 30 : 15, if complete carbonate decomposition is attained.

The XRD pattern of the calcined CZA catalyst is shown in Fig. 1 (graph B). The peaks could be assigned to CuO (30) and ZnO (31) phases. The broad XRD peaks indicate that the Cu and Zn oxides are ill-defined crystalline phases, as one would expect for a good Cu-based methanol synthesis catalyst. Similar results have been reported by different authors for other CuO–ZnO-based catalysts prepared under similar conditions (32, 33).

The nature and precise arrangement of the CO_3^{2-} units remaining in the CZA mixed oxide, due to the incomplete Cu–Zn hydrotalcite decomposition, have not been thoroughly examined in the literature. In fact, no Cu–Zn carbonate was detected by XRD, which indicates that the phase must be amorphous. However, it is believed that the thermally induced changes in the hydrotalcite-like compounds take place through a topotactic decomposition of the brucite-like layers. Such a process gives an oxycarbonate in which the metal–oxygen framework remains essentially intact and the carbonate anions are still retained in the interlayer region.

The XRD patterns of the calcined Pd-containing catalysts are represented in Fig. 1 [patterns C (4Pd/CZA) and D (10Pd/CZA)]. At first glance these profiles seem to be very similar to that of the calcined CZA sample. Closer examination, however, shows that the CuO peaks are sharper for the modified catalysts in comparison to CZA whereas the ZnO peaks remain essentially unchanged. Since the width of an XRD peak is related to the size of the crystallites, it is concluded that the sharper the CuO diffraction peaks, the bigger the CuO average size of the particle distribution. The crystallite size of the CuO phase can be quantitatively estimated by the line broadening of the (111) diffraction line at $2\theta \approx 38.77^\circ$ by applying the Scherrer equation (see Experimental). The Scherrer equation should not be used for absolute determinations due to its failure to account for the particle size distribution and the uncertainty in correcting for instrumental line broadening. Despite this fact, however, the calculations are useful as a relative measure of average crystallite size. The values obtained are listed in Table 2 and indicate that the CuO crystal sizes for the calcined Pd-containing catalysts are larger than those for the CZA sample. In the case of sample 10Pd/CZA, a weak peak at $2\theta \approx 33.84^\circ$, which is partially overlapped with CuO and ZnO contributions, appeared upon using a slower scanning rate in the range $30^\circ < 2\theta < 45^\circ$ (see top profile in Fig. 1). This feature points to incipient formation of PdO crystallites. The absence of clear evidence for the presence of PdO in 4Pd/CZA indicates that the PdO phase is rather well dispersed over the surface of the calcined CZA. The PdO crystallites are detected only for higher loadings.

TABLE 2

Average CuO Crystal Size and BET Area for Calcined Catalysts, and Amount of Exposed Copper for Reduced Catalysts

Catalyst	XRD crystal size D_{CuO} (nm)	BET area (m^2/g)	Pulse-N_2O Chem. Exposed copper[a] (μmol Cu_S/g_{cat})
CZA	8.1	39.5	359.0 (14.8)
4Pd/CZA	10.8	31.8	202.0 (8.3)
10Pd/CZA	11.0	30.1	137.0 (5.6)

[a] Values in parentheses represent square meters of copper per gram of catalyst (m^2Cu/g_{cat}) assuming 1.46×10^{19} Cu atoms/m^2. The experimental error was within ±3%.

TABLE 3

Summary of TPR Data for Calcined Samples

Catalyst	K (sec)[a]	P (K)[a]	T_M (K)[b]	H_2/M[c]
CZA	142.5	23.8	496	1.16
4Pd/CZA	58.9	9.9	346 (13.2) 403 (34.8) 456 (52.0)	1.28
10Pd/CZA	74.3	12.4	348 (26.6) 379 (25.6) 442 (47.8)	1.30

[a] $K = S_o/(V^*C_o)$ and $P = \beta S_o/(V^*C_o)$ where S_o is the initial amount of reducible oxide species (μmole), C_o is the initial hydrogen concentration (μmole mL^{-1}), V^* is the total flow rate (mL sec^{-1}), and β is the heating rate (K sec^{-1}).

[b] Values in parentheses represent the percentage of each peak with respect to the total area.

[c] The experimental error for the H_2 consumed was ±5%.

The specific BET areas of the calcined catalysts are given in Table 2. A marked decrease in the specific area is observed when Pd is added to the base calcined CZA. Furthermore, the decreases in the BET areas for the two Pd-modified catalysts are almost equal. The increase in the average CuO crystal size could explain the lower BET area found for the Pd-modified samples.

TPR experiments were carried out not only to determine the optimal catalyst activation conditions but also to investigate the interaction between Pd and Cu metals in the catalytic systems. The main parameters of the TPR measurements are listed in Table 3. The parameters K and P (see Table 3 for definitions), which were introduced by Monti and Baiker (23) and Malet and Caballero (24), respectively, are very helpful in establishing the optimum conditions to perform the TPR experiments. Selection of the appropriate conditions guarantees that the TPR peak position and the resolution of the different reduction processes are not affected by experimental conditions. The criteria state that the characteristic K parameter must lie between 55 and 140 sec (for heating rates between 6 and 18 K/min), whereas the P value must be lower than ca. 20 K. As shown by the values in Table 3, the K and P parameters fulfill the aforementioned criteria for all the catalysts. The results derived from the TPR experiments are therefore reliable and are not affected by the operating variables.

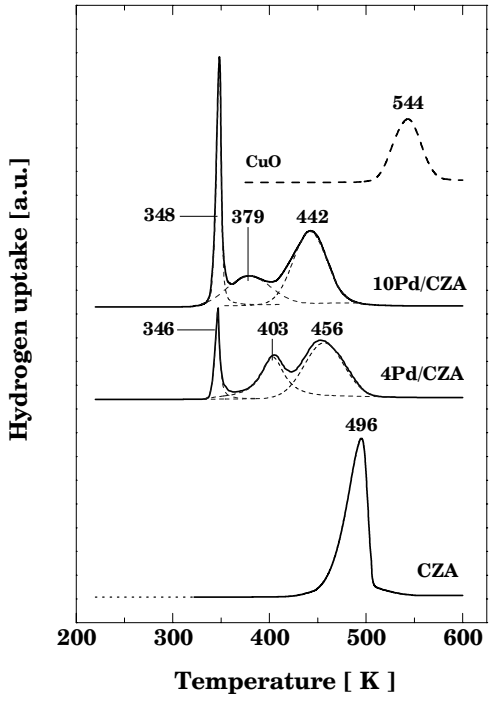

FIG. 3. TPR profiles for calcined samples and pure CuO as reference compound.

The TPR profiles of the catalysts are represented in Fig. 3 along with that of CuO as a reference compound. The profile of the calcined CZA sample shows only one reduction peak, centred at 496 K, which was assigned to the reduction of CuO to Cu : $CuO + H_2 \rightarrow Cu^0 + H_2O$. Although the reduction of bulk ZnO is thermodynamically feasible at high temperatures, ZnO was not reduced under our experimental conditions. However, partial reduction of surface ZnO, which may lead to the formation of α-brass (i.e., a dilute alloy of zinc in copper) only few layers thick on the copper crystallites during catalyst reduction, cannot be ruled out. In fact, detailed thermodynamic calculations (34) are in favor of such a hypothesis, showing that the equilibrium zinc content in a surface α-brass is about 5% during catalyst reduction at 573 K. The shape of this reduction peak, which is asymmetric with a tail towards lower temperatures, may be the result of a complex overlapping of several elemental reduction processes arising from different Cu(II) species. In this context, it is known that CuO–ZnO-based catalysts are heterogeneous in terms of the CuO particle size and the Cu(II) short-range environment (35–39). The presence of only one peak for the reduction of CuO in the CZA sample is in accordance with the literature data, but the T_M value is different compared to that of the CuO reference compound. The peak was displaced by almost 50 K towards lower temperatures with respect to the CuO reference. This result indicates that ZnO enhances the reducibility of the copper phase, a fact that is consistent with previous observations (40).

The ratio between the amount of hydrogen consumed and the amount of reducible oxide species present (H_2/M in Table 3) was determined quantitatively. According to the stoichiometry of the CuO reduction, this ratio should have a value of one. An experimental value higher than the theoretical one was obtained for the CZA catalyst, $(H_2/M)_{EXP} = 1.16$, which is too high to be ascribed to the experimental error inherent in this technique (up to 5%). It is widely accepted that both ZnO and copper crystallites are capable of occluding large amounts of hydrogen both on the surface and in subsurface regions (41, 42). This additional quantity of hydrogen, whether adsorbed on the surface or stored in the ZnO crystalline structure, could explain the increase in the $(H_2/M)_{EXP}$ value found for the CZA sample.

The addition of palladium to the base CZA causes dramatic changes in the TPR profiles. First, the profiles consist of three different peaks that must correspond to different reduction processes, as shown by applying curve deconvolution procedures (dashed lines in Fig. 3). Second, the H_2/M ratios for these Pd-modified samples, where the M value now accounts for both PdO- and CuO-reducible oxides, are higher than those for the base CZA catalyst (see Table 3). This finding is interpreted as an evidence of the ease with which hydrogen is dissociated on Pd particles and then spilt over the Cu–ZnO–Al_2O_3 phases. This spilling of hydrogen results in an increase in hydrogen consumption, regardless of whether it is adsorbed on the surface or stored in the ZnO crystalline structure. In addition, it could also be expected that formation of a Cu–Zn alloy is aided by H_2 spillover from Pd particles.

As mentioned earlier, the TPR profiles for the Pd-modified systems consist of three reduction peaks. These reduction processes occur at lower temperatures than for CZA, which indicates that the reducibility of CuO is enhanced by the presence of palladium. It seems reasonable to assign the first peak, which appears at about 350 K, to PdO reduction because the peak area increases with the Pd loading. However, it has been shown that isolated PdO particles are reduced at temperatures lower than room temperature and display a negative peak close to room temperature attributed to hydrogen desorption from decomposition of Pd hydrides (43). Since neither of these features is observed in the TPR profiles for the Pd-modified catalysts, the PdO phase must be well dispersed over the CuO–ZnO–Al_2O_3 phases. Furthermore, the hydrogen consumption at 350 K exceeds the stoichiometric amount needed for the complete reduction of PdO. For informative purposes, the experimental H_2/M ratio for the 4Pd/CZA sample at 350 K is 0.17, which represents almost 3.5 times the stoichiometric value for the whole PdO reduction. This indicates that the low-temperature reduction peak not only corresponds to PdO reduction ($PdO + H_2 \rightarrow Pd + H_2O$) but also to partial CuO reduction.

The two subsequent reduction processes are assigned to the reduction of the remaining CuO to Cu. Both peaks are shifted to lower temperatures with respect to the CZA catalyst. This shift in the CuO reduction in Pd-containing CuO–ZnO-based catalysts has scarcely been reported in the literature but is generally interpreted as being due to a Pd–Cu interaction. It is accepted, for bimetallic Pd–Cu systems, that the palladium sites that are reduced first act as sink for H_2, which once activated is spilt over the neighbouring phases. Given this property of palladium metal, it is reasonable to assume that palladium is performing its function in the reduction of CuO in two ways: (i) acting as new nucleation center and/or (ii) providing a high concentration of active hydrogen that is susceptible for use in CuO reduction. Whatever the mechanism, whether pure or combined, the reduction of CuO will be facilitated.

3.3. Characterisation and Catalytic Activity of the Reduced Catalysts

N_2O chemisorption measurements. The amount of exposed copper in the reduced catalysts, as determined by pulsed-N_2O chemisorption, is given in Table 2. This parameter is very important in Cu-based methanol-synthesis catalysts since it has been shown that there is a linear relationship between the methanol yield of such catalysts and their copper surface area (1, 3). The values given in this study were obtained empirically by quantifying the amount of N_2O reacted with the Cu surface atoms according to the method described in the Experimental section.

Nonetheless, it is possible that noble metals, such as palladium, are capable of consuming N_2O. In fact, a 2% PdO/ZnO reference sample prepared by wetness impregnation ($S_{BET} = 9.6\ m^2/g$) exhibited an N_2O consumption of 13.4 μmol N_2O/g_{cat}. Similar results have been reported for zirconia-supported silver catalysts (44). This fact represents a serious interference in the determination of the real amount of exposed copper, and is considered in the discussion following. However, it should be emphasized that such a palladium interference leading to an overestimation in the amount of exposed copper does not affect the conclusions presented in the following section.

The impregnation of the base CZA catalyst resulted in a substantial decrease in the amount of N_2O consumed. This consumption is due to the exposed copper and in part to surface palladium atoms. In connection with the XRD analysis of the calcined catalysts, the observed increase in the CuO crystal size corresponds to the decrease in the copper surface area for the reduced Pd-containing catalysts. In other words, larger CuO particles result in larger Cu metal particles after reduction. The decrease in the amount of exposed copper for the reduced catalyst 10Pd/CZA is much greater than for the reduced catalyst 4Pd/CZA. The fact that both modified catalysts have a similar BET surface area leads us to believe that the low amount of exposed copper for the 10Pd/CZA catalyst can be explained by the larger amount of palladium added to the base CZA catalyst. This large amount of noble metal physically occludes the copper particles, which in turn results in a decrease in the amount of exposed copper. Another possibility involves the formation of bimetallic PdCu aggregates with the subsequent development of a Pd–Cu alloy. With regard to the latter possibility, the formation of a Pd–Cu alloy has been reported for catalysts prepared by co-impregnation of Cu and Pd salts after calcination and activation under hydrogen (45–47). Therefore, under the catalyst preparation and activation conditions used here, the development of a Pd–Cu alloy, a process that results in dilution of the surface copper atoms and hence a decrease in the copper surface area, is expected to occur to some extent.

These two hypotheses, advanced to explain the extra depletion of the amount of exposed copper for the 10Pd/CZA catalyst, are supported by the assumption that palladium does not consume as much N_2O as copper. Otherwise, the explanation must be obtained by assuming that the sintering phenomena of copper is taking place during the reduction step induced by the high loading of palladium. As this noble metal enhances the reduction of CuO, the sintering of Cu particles is expected to occur at temperatures around 553 K.

Finally, if a comparison is made between the decrease of exposed copper between CZA and 4Pd/CZA catalysts with the increase of the square CuO particle sizes (D^2_{CuO}), the values obtained are quite similar. Consistently, the growth of CuO particle size could explain the partial depletion of copper surface area. The term partial depletion is used here because the 10Pd/CZA catalyst suffers an extra abatement, previously discussed in terms of the high amount of palladium added. A detailed study about the causes of such enlargement of the CuO particles, upon palladium incorporation, will be presented in Sect. 3.4.

Catalytic performance in methanol synthesis from CO_2/H_2. The catalytic activity of the reduced catalysts in the hydrogenation of CO_2 was tested. Methanol was the main product (reaction [1]) but CO formation took place simultaneously by the reverse water gas shift (RWGS) side reaction (reaction [2]). Small traces of methane were also detected at high temperatures. The selectivity to MeOH is therefore defined as the ratio of the amount of CO_2 converted to MeOH to the amount of CO_2 converted to MeOH and CO. The methanol yield (MTY), expressed as mol MeOH/(h kg_{cat}), is displayed as a function of reaction temperature in Fig. 4 (graph A). The methanol yield was found to increase with increasing temperature, without any decreasing or limiting value, indicating that thermodynamic restrictions or diffusion limitations were absent. For informative purposes, the thermodynamic limit of MTY is also included in Fig. 4 (graph A). In addition, CO production was found to increase faster than the MTY with temperature, thus causing a decrease in the methanol selectivity with

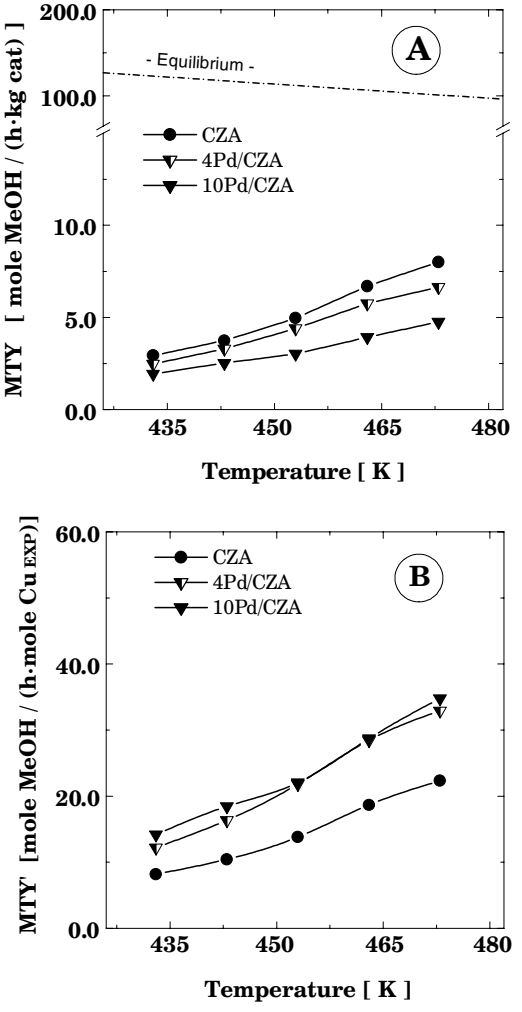

FIG. 4. (A) Methanol yield [mol MeOH/(h kg_{cat})] and (B) intrinsic methanol yield [mol MeOH/(h mole Cu_{EXP})] as a function of the reaction temperature for the catalysts. Conditions: $P = 40$ bar, $CO_2/H_2 = 3$, $W/F = 0.042$ kg · h/m^3, and $T = 433$–473 K. The dashed line in (A) indicates the thermodynamic yield of methanol at 40 bar.

temperature and hence with CO_2 conversion. This result is shown in Fig. 5 (graph B), where the methanol selectivity is seen to decrease with CO_2 conversion. This higher thermal dependence for CO formation agrees with the higher apparent activation energy for the RWGS reaction in comparison to methanol synthesis, as reported in the literature (48, 49).

Pd-containing catalysts show a significant decrease in the MTY with respect to the base CZA catalyst (Fig. 4 [graph A]). The addition of Pd does not appear to promote the methanol yield. Indeed, the presence of Pd seems to lower the activity of the catalyst, in contrast to the results reported for other Pd-modified Cu–Zn systems (7–9). This lowering of the MTY can be ascribed to a decrease in the CO_2 conversion and/or a decrease in the selectivity towards methanol. The conversion of CO_2 for Pd-containing catalysts was lower than for the CZA counterpart at all temperatures (Fig. 5 [graph A]), and decreased with Pd loading. However, the methanol selectivity versus CO_2 conversion (Fig. 5 [graph B]) was quite similar for all the catalysts. These trends indicate that the decrease in the MTY comes from a loss of catalyst activity and not from a loss in selectivity of the active centers.

Bearing in mind that the active sites involved in the formation of methanol require surface copper, the former definition of MTY, i.e., [mol MeOH/(h kg_{cat})], is not appropriate for use in showing the promotion effect of Pd since the palladium-modified catalysts are associated with a marked decrease in the copper surface area. A more suitable representation is depicted in Fig. 4 (graph B). This figure shows the intrinsic methanol yield [mol MeOH/(h mol Cu_{EXP})], expressed per mole of exposed copper determined

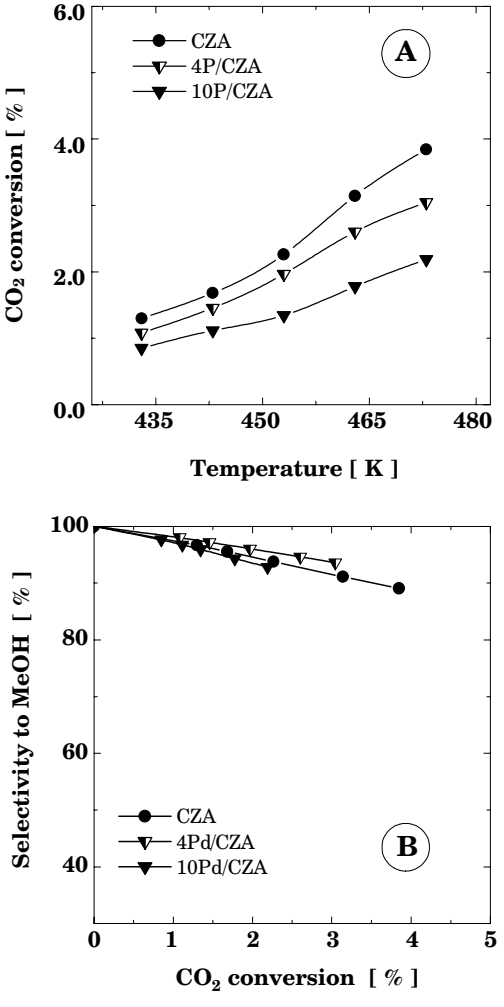

FIG. 5. (A) Carbon dioxide conversion (%) as a function of the reaction temperature and (B) methanol selectivity (%) against CO_2 conversion (%).

by pulse-N_2O chemisorption, as a function of the reaction temperature. It can be seen that the intrinsic yields of methanol for the two Pd-containing catalysts are very similar and substantially higher than that obtained with the nonpromoted catalyst. The promotion in methanol formation was independent of the palladium loading, suggesting that Pd in effect may already have reached saturation. The addition of a certain amount of Pd to the CZA base catalyst has a beneficial effect on the methanol synthesis—in terms of intrinsic MTY—but the addition of Pd beyond this level does not provide any further advantage. Therefore, the 10Pd/CZA catalyst must be considered as a model system, where the beneficial effect of palladium over the copper species should be more evident by the characterisation techniques used. This belief is further evidenced by the enhancement of both the CuO reducibility and the H_2/M ratio for the 10Pd/CZA catalyst, with respect to the catalyst 4Pd/CZA.

These trends of the intrinsic methanol yield also suggest that Pd does not act as an independent catalytic site for methanol synthesis, because the observed promotion is independent of the metal loading. In this context, Gotti and Prins, in contrast to previous claims, demonstrated that Pd is worse than Cu for CO_2 hydrogenation to methanol (50).

In regard to the results of N_2O chemisorption, since palladium partially reacts with N_2O, the real amount of exposed copper is lower than the value already estimated by the pulsed-chemisorption technique. Consequently, the intrinsic methanol yield of the Pd-modified catalysts would be even higher, a situation that provides further support for the promoting effect of palladium.

In spite of the previous comment, we have to be rather careful with such results about the intrinsic promoting effect of palladium. The real amount of exposed copper is unknown due to the palladium interference during the N_2O chemisorption measurements. Thus, the intrinsic MTY comprises some uncertainty and the true promotion by palladium cannot be determined by the techniques applied. Therefore, the values of the promotion given in Fig. 4 (graph B) may be considered in a qualitative manner, even though the effect of the noble metal is evident.

As far as the promoting effect of palladium in modified methanol synthesis catalysts is concerned, it has been claimed that Pd enhances the concentration of hydrogen available on the active centers by means of H_2 spillover (7–9). This process improves the rate-limiting step of the reaction mechanism (formate hydrogenolysis) and furthermore, the copper surface is kept in a more reduced state, which counteracts the oxidising effect of the CO_2 and/or H_2O byproduct. The increase of the H_2 consumed, as revealed by TPR experiments, points to the proposed H_2-spillover mechanism as being responsible for the increase in the intrinsic methanol yield. However, another possible mechanism of promotion on the working Pd-modified catalysts cannot be ruled out. In a recent work (51) we stated that the increase in the methanol yield for Pd–Cu–Zn-based catalysts might not be explained on the basis of a single phenomenon. By means of H_2–CO_2–H_2 redox cycles, a novel mechanism was proposed in which Pd, either by an "ensemble" or "ligand effect" (52), modifies the surface redox properties of Cu. Both the H_2 spillover and the stabilisation of Cu against CO_2 oxidation (hypothesis of Pd–Cu alloy formation) have been suggested to contribute to the enhancement of the methanol yield in Pd-modified Cu–Zn catalysts (51).

3.4. Rehydration of the Base CZA Calcined Catalyst

The previous section reveals that the decrease in the amount of exposed copper results in an apparent masking of the promoting effect of palladium in terms of grams of catalyst. This masking effect is due to the larger CuO particles formed, as was already suggested in Sect. 3.3. An explanation for the increase in the CuO particle size for the Pd-modified catalysts is still required.

It is known that the hydrothermal treatment of *ex* hydrotalcite mixed oxides can lead to the regeneration of the original hydrotalcite structure (memory effect) (53, 54). In general, this memory effect depends on the formulation of the parent hydrotalcite, the calcination temperature, and the conditions of the regeneration (temperature, atmosphere, and time). Such rehydrated hydrotalcite-containing oxides must be calcined again before they can be used as modified catalysts. However, such structural reversibility, at the intermediate level of catalyst preparation, is often detrimental to the catalytic activity. It was reported that hydrotalcite reconstruction induces segregation of phases from the mixed oxides, leading to inhomogeneous and low-specific-area final mixed oxides (55). For example, Nunan *et al.* reported that hydration plays an important role in the preparation of alkali metal-doped methanol synthesis catalysts (56).

Given the points just outlined, it is not surprising that similar phenomena take place in our Cu–Zn–Al mixed oxide during wet palladium impregnation. In an attempt to confirm this hypothesis, a blank experiment was carried out on the base CZA catalyst, whereby the sample was subjected to the aforementioned aqueous impregnation procedure without the presence of the palladium precursor in the aqueous solution. The solid obtained in this way was dried again at 393 K and recalcined at 673 K.

Figure 6 shows the XRD pattern of the calcined CZA base catalyst along with those of the materials obtained by rehydration (rehydrated CZA) and after calcination (recalcined CZA). It is shown that the rehydrated-CZA material displays the characteristic peaks due to the CuO and ZnO phases as well as the typical pattern of the Cu–Zn hydrotalcite-like structure, which proves that the hydrotalcite phase has been partially regenerated. The presence of

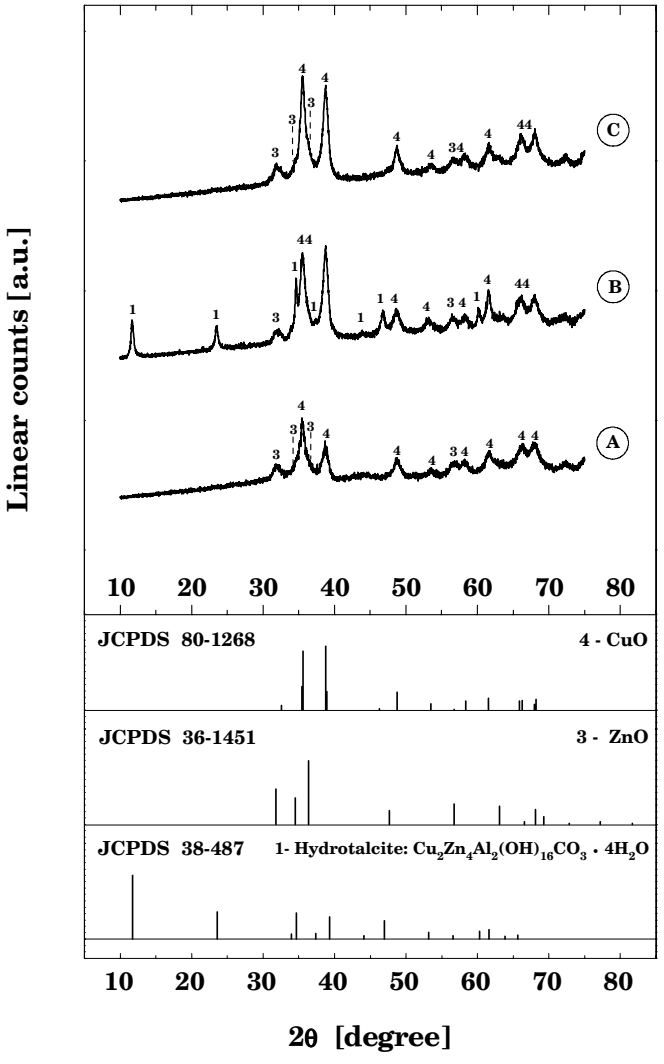

FIG. 6. X-ray powder diffraction profiles for (A) CZA calcined catalyst, (B) rehydrated-CZA, and (C) final recalcined-CZA materials.

remaining CO_3^{2-} anions in the CZA catalyst and the thermal treatment with water in a rotary evaporator (i.e., a hydrothermal-like treatment) allow the partial reconstruction of the initial lamellar Cu–Zn hydrotalcite-type structure (memory effect). It is believed that the hydrotalcite regeneration is facilitated by hydrotalcite thermal decomposition that occurs through a topotactic process, where the CO_3^{2-} anions are still retained in the interlayer region of the oxycarbonate and the metal–oxygen framework remains essentially intact. In fact, recent studies (57, 58) suggest that the reformation occurs via a retrotopotactic transformation, i.e., a reverse topotactic transformation. On the other hand, the CuO diffraction peaks for rehydrated CZA are narrower than those for calcined CZA, whereas ZnO does not show an enhancement in the crystallinity. Consequently, the hydrothermal-like treatment gives rise to hydrotalcite restoration as well as growth of the CuO particles. When the latter sample was calcined (recalcined CZA), the hydrotalcite decomposed to give the corresponding metal oxides and, consequently, only CuO and ZnO peaks were detected. A high CuO crystallinity is maintained in this material.

The mean crystallite sizes of CuO and ZnO for these materials were calculated using the Scherrer equation and the values obtained are given in Table 4. The CuO crystal size of the rehydrated-CZA sample was higher by almost 40% than that of the base CZA sample. The fact that the crystallite size for the recalcined-CZA material is similar to that of the rehydrated-CZA material clearly indicates that the increase of CuO crystallinity results from the hydrothermal-like treatment and not from the further recalcination. The crystal size of the ZnO phase remains practically unaffected in all cases. In addition, the enhancement in the CuO particle size is accompanied by a decrease in the BET area (Table 4).

When the preceding results are compared with those of the Pd-modified catalysts, the similarity between the systems is evident. The average CuO particle sizes and BET surface areas for the Pd-modified catalysts are very similar to those of the recalcined-CZA sample. This leads us to conclude that the increase in the CuO crystallinity found for the modified Pd/CZA samples is caused by the hydrothermal-like treatment during the wet Pd-impregnation step. In addition to the hydrotalcite reconstruction, a rearrangement of the CuO phase takes place that results in larger CuO crystallites.

In connection with the preceding observation, several authors have already reported induced phenomena during the hydrotalcite reconstruction in mixed oxides. Kooli *et al.* found an improvement in ZnO crystallinity during the rehydration of Zn–Al layered double hydroxides (59). Hibino and Tsunashima demonstrated the segregation of aluminium from the structure upon performing calcination and reconstruction cycles on Mg–Al–CO_3 hydrotalcite (60). The same authors also reported an improvement in Mg–Fe spinel formation due to hydration/calcination cycles in Mg–Fe–CO_3 hydrotalcites (61). In terms of our system, we suggest that the migration of water plays a key role in the

TABLE 4

BET Area and Average Crystal Size (CuO and ZnO) for the CZA Calcined Catalyst and Derived Materials

Catalyst	BET area (m^2/g)	XRD crystal size (nm)	
		D_{CuO}	D_{ZnO}
CZA	39.5	8.1	7.3
Rehydrated CZA	24.9	11.3	7.8
Recalcined CZA	33.6	11.3	7.8

reconstruction process. The ability of water molecules to diffuse into the carbonate-modified CuO–ZnO–Al_2O_3 oxide and reconstruct the hydrotalcite would cause the growth of CuO crystallites by coalescence. Although a more detailed study is needed to confirm such a hypothesis and provide a definitive interpretation, this coalescence concept for copper-oxide-containing materials has already been introduced by Fujita *et al.* (62) to explain the effect of the calcination heating rate on the CuO phase crystallinity for CuO–ZnO-based materials.

4. CONCLUSIONS

The retention of carbonate anions in the calcined CZA catalyst, which is due to the incomplete decomposition of the Cu–Zn hydrotalcite-like phase, has significant implications for the subsequent wet palladium impregnation. The hydrothermal-like treatment of the carbonate-containing CZA mixed oxide during the Pd-impregnation step allows the partial reconstruction of the original Cu–Zn hydrotalcite phase. In addition, an enhancement of the CuO phase crystallinity is observed as a consequence of a crystalline rearrangement of this oxidic phase during the hydrotalcite reconstruction. This rearrangement, and consequent loss of copper dispersion in the reduced Pd-modified catalysts, results in the hindrance of the promoting effect of palladium for the catalyst performance in methanol synthesis by hydrogenation of CO_2. Nitrous oxide chemisorption measurements allow the redefinition of the methanol yield per mole of exposed copper, a situation that reveals a certain promoting effect of palladium in qualitative terms, since palladium interferes with the evaluation of the amount of exposed copper and the actual promotion by palladium is unknown. TPR experiments show that the presence of palladium metal improves the reducibility of copper oxide. The appearance of low-temperature reduction peaks and the increase in the hydrogen consumption for the Pd-modified catalysts, compared to the base CZA catalyst, support the proposed H_2-spillover mechanism as being responsible for the increase in the intrinsic methanol yield.

ACKNOWLEDGMENTS

This work was supported by CICYT (Spain) under Grant QUI98-0877. I. Melián-Cabrera thanks the Ministry of Education and Science for a fellowship.

REFERENCES

1. Chinchen, G. C., Mansfield, K., and Spencer, M. S., *CHEMTECH* **Nov**., 692 (1990).
2. Kagan, Y. B., Liberov, L. G., Slivinskii, E. V., Loktev, S. M., Lin, G. I., Rozovskii, A. Y., and Bashkirov, A. N., *Dokl. Akad. Nauk SSSR* **221**, 1093 (1975).
3. Chinchen, G. C., Denny, P. J., Parker, D. G., and Spencer, M. S., *Appl. Catal.* **30**, 333 (1987).
4. Bowker, M., Hadden, R. A., Houghton, H., Hyland, J. N. K., and Waugh, K. C., *J. Catal.* **109**, 263 (1988).
5. Inui, T., Hara, H., Takeguchi, T., and Kim, J. B., *Catal. Today* **36**, 25 (1997).
6. Saito, M., Fujitani, T., Takeuchi, M., and Watanabe, T., *Appl. Catal. A* **138**, 311 (1996).
7. Inui, T., and Takeguchi, T., *Catal. Today* **10**, 95 (1991).
8. Fujimoto, K., and Yu, Y., *Stud. Surf. Sci. Catal.* **77**, 393 (1993).
9. Sahibzada, M., Chadwick, D., and Metcalfe, I. S., *Catal. Today* **29**, 367 (1996).
10. Chinchen, G. C., Waugh, K. C., and Whan, D. A., *Appl. Catal.* **25**, 101 (1986).
11. Denise, B., Sneeden, R. P. A., Beguin, B., and Cherifi, O., *Appl. Catal.* **30**, 353 (1987).
12. Tagawa, T., Pleizier, G., and Amenomiya, Y., *Appl. Catal.* **18**, 285 (1985).
13. Amenomiya, Y., *Appl. Catal.* **30**, 57 (1987).
14. Koeppel, R. A., Baiker, A., Schild, C., and Wokaun, W., *Stud. Surf. Sci. Catal.* **63**, 59 (1991).
15. Kanoun, N., Astier, M. P., and Pajonk, G. M., *Catal. Lett.* **15**, 231 (1992).
16. Walker, A. P., Lambert, R. M., Nix, R. M., and Jennings, J. R., *J. Catal.* **138**, 694 (1992).
17. Barrault, J., Rassoul, Z., and Bettahar, M. M., *Stud. Surf. Sci. Catal.* **61**, 367 (1991).
18. Arakawa, H., Sayama, K., Okabe, K., and Murakami, A., *Stud. Surf. Sci. Catal.* **77**, 389 (1993).
19. Fujitani, T., Saito, M., Kanai, Y., Kakumoto, T., Watanabe, T., Nakamura, J., and Uchijima, T., *Catal. Lett.* **25**, 271 (1994).
20. Toyir, J., de la Piscina, P. R., Fierro, J. L. G., and Homs, N., *Appl. Catal. B* **29**, 207 (2001).
21. Melián-Cabrera, I., López Granados, M., Terreros, P., and Fierro, J. L. G., *Catal. Today* **45**, 251 (1998).
22. Li, J. L., and Inui, T., *Appl. Catal., A* **137**, 105 (1996).
23. Monti, D. A. M., and Baiker, A., *J. Catal.* **83**, 323 (1983).
24. Malet, P., and Caballero, A., *J. Chem. Soc., Faraday Trans. 1* **84–7**, 2369 (1988).
25. Evans, J. W., Wainwright, M. S., Bridgewater, A. J., and Young, D. J., *Appl. Catal.* **7**, 75 (1983).
26. Dell, R. M., Stone, F. S., and Tiley, P. F., *Trans. Faraday Soc.* **49**, 195 (1953).
27. X-ray Powder Data File, JCPDS 38-487.
28. X-ray Powder Data File, JCPDS 36-1475.
29. Gherardi, P., Ruggeri, O., Trifiró, F., Vaccari, A., del Piero, G., Manara, G., and Notari, B., *Stud. Surf. Sci. Catal.* **16**, 723 (1983).
30. X-ray Powder Data File, JCPDS 80-1268.
31. X-ray Powder Data File, JCPDS 36-1451.
32. Alejo, L., Lago, R., Peña, M. A., and Fierro, J. L. G., *Appl. Catal.* **162**, 281 (1997).
33. Figueiredo, R. T., Martínez-Arias, A., López Granados, M., and Fierro, J. L. G., *J. Catal.* **178**, 146 (1998).
34. Spencer, M. S., *Surf. Sci.* **192**, 323, 329, 336 (1987).
35. Okamoto, Y., Fukino, K., Imanaka, T., and Teranishi, S., *J. Phys. Chem.* **87**, 3740 (1983).
36. Garbassi, F., and Petrini, G., *J. Catal.* **90**, 106 (1984).
37. Garbassi, F., and Petrini, G., *J. Catal.* **90**, 113 (1984).
38. Moretti, G., Lo Jacono, M., Fierro, G., and Minelli, G., *Surf. Interface Anal.* **9**, 246 (1986).
39. Moretti, G., Fierro, G., Lo Jacono, M., and Porta, P., *Surf. Interface Anal.* **14**, 325 (1989).
40. Fierro, G., Lo Jacono, M., Inversi, M., Porta, P., Cioci, F., and Lavecchia, R., *Appl. Catal. A* **137**, 327 (1996).
41. Waugh, K. C., *Catal. Today* **15**, 51 (1992).
42. Bailey, S., and Waugh, K. C., *Catal. Lett.* **17**, 371 (1993).
43. Chang, T. C., Chen, J. J., and Yeh, C. T., *J. Catal.* **96**, 51 (1985).

44. Fröhlich, C., Köppel, R. A., Baiker, A., Kilo, M., and Wokaun, A., *Appl. Catal.*, *A* **106**, 275 (1993).
45. Toshima, N., and Wang, Y., *Langmuir* **10**, 4574 (1994).
46. Fernández García, M., Anderson, J. A., and Haller, G. L., *J. Phys. Chem.* **100**, 16247 (1996).
47. Furlong, B. K., Hightower, J. W., Chan, T. Y. L., Sarkany, A., and Guczi, L., *Appl. Catal*. **117**, 41 (1994).
48. Yoshihara, J., Parker, S. C., Schafer, A., and Campbell, C. T., *Catal. Lett.* **31**, 313 (1995).
49. Ovensen, C. V., Clausen, B. S., Schiøtz, J., Stoltze, P., Topsøe, H., and Nørskov, J. K., *J. Catal.* **168**, 133 (1997).
50. Gotti, A., and Prins, R., *J. Catal.* **175**, 302 (1998).
51. Melián-Cabrera, I., López Granados, M., and Fierro, J. L. G., *Catal. Lett.* **79**, 165 (2002).
52. Nonneman, L. E. Y., and Ponec, V., *Catal. Lett.* **7**, 197 (1990).
53. Miyata, S., *Clays Clay Miner.* **28**, 50 (1980).
54. Sato, T., Kato, K., Endo, T., and Shimada, M., *React. Solids* **2**, 253 (1986).
55. Courty, Ph., and Marcilly, Ch., *Stud. Surf. Sci. Catal*. **16**, 485 (1983).
56. Nunan, J. G., Himelfarb, P. B., Herman, R. G., Klier, K., Bogdan, C. E., and Simmons, G. W., *Inorg. Chem.* **28**, 3868 (1989).
57. Marchi, A. J., and Apesteguía, C. R., *Appl. Clay Sci.* **13**, 35 (1998).
58. Pérez-Ramírez, J., Mul, G., Kapteijn, F., and Moulijn, J. A., *Mater. Res. Bull.* **36**, 1767 (2001).
59. Kooli, F., Depège, C., Ennaqadi, A., de Roy, A., and Besse, J. P., *Clays Clay Miner.* **45**, 92 (1997).
60. Hibino, T., and Tsunashima, A., *Chem. Mater.* **10**, 4055 (1998).
61. Hibino, T., and Tsunashima, A., *J. Mater. Sci. Lett*. **19**, 1403 (2000).
62. Fujita, S., Moribe, S., Kanamori, Y., Kakudate, M., and Takezawa, N., *Appl. Catal.*, *A* **207**, 121 (2001).